ASTRA-BF: A Human-in-the-loop Algorithm for Predicting Surface Transitions in Robotic Lower Limb Prosthetics Using Biomechanical Features

Charikleia Angelidou[a], Jaclyn M. Sions[b], Panagiotis Artemiadis[c,*]

[a]*Department of Mechanical Engineering, University of Delaware, 210 S College Ave, 19716, Newark, DE, USA*
[b]*Department of Physical Therapy, University of Delaware, 210 S College Ave, 19716, Newark, DE, USA*
[c]*Department of Mechanical Engineering, University of Delaware, 210 S College Ave, 19716, Newark, DE, USA*

Abstract

In the realm of lower-limb prosthetics and wearable devices, the significance of walking on compliant surfaces for individuals with lower-limb amputations (LLA) cannot be overstated. The interaction between humans and compliant surfaces presents a unique challenge, particularly for those relying on prosthetic interventions. Ensuring the safety, stability, and fluidity of movement on these surfaces is paramount for preventing falls in this population. This work delves into the critical importance of addressing this challenge, outlining the complexities involved in walking on compliant surfaces, and exploring high-level control strategy interventions aimed at mitigating the inherent difficulties faced by individuals with LLA. We specifically expand on an individualized pattern recognition (PR) and classification approach utilizing kinematic, kinetic, and surface electromyography (EMG) data to discern user intent for transitioning from rigid to compliant surfaces of variable stiffness. This work proposes an efficient Algorithm for Surface TRAnsition prediction in robotic lower limb prosthetics using Biomechanical Features,

⋆This material is based upon work supported by the National Science Foundation under Grants No. 2020009, 2015786, 2025797, and 2018905.

*Corresponding author

Email addresses: cangelid@udel.edu (Charikleia Angelidou), megsions@udel.edu (Jaclyn M. Sions), partem@udel.edu (Panagiotis Artemiadis)

called ASTRA-BF. Integrating a k-Nearest Neighbors (kNN) methodology alongside a Naive Bayes classification, our strategy can accurately forecast impending transitions in four different levels of surface stiffness in real time. This capability enables swift parameter control of prostheses or wearable devices, facilitating adaptation to diverse terrains. Post-implementation of the ASTRA-BF, classification results attain a prediction accuracy of up to 82%, demonstrating the feasibility and efficiency of real-time prediction for transitions to various compliant surfaces in both healthy and clinical populations. The proposed framework has the potential to propel the field of robotics toward novel solutions that not only enhance mobility but also significantly improve the quality of life for those navigating the intricate terrain of compliant surfaces with prosthetic limbs.

Keywords: lower-limb prostheses, human-in-the-loop, prostheses control, compliant surfaces, surface prediction, multi-class classification

1. Introduction

The ability to walk seamlessly and securely on various terrains is a fundamental aspect of human mobility, facilitating independence and active participation in daily life. Walking on compliant terrain is particularly challenging because the surfaces are typically uneven and non-uniform. The characteristics of compliant terrain, as well as the transitions between surfaces of varying stiffness, make the fulfillment of task demands particularly challenging [1]. The mechanical properties of compliant surfaces, characterized by their deformability and variability, introduce a layer of complexity that calls for innovative solutions in the domain of artificial or robotic walkers, such as in lower-limb prosthetic interventions.

Specifically for individuals with lower-limb amputations (LLA), the pursuit of a stable and natural gait pattern becomes markedly challenging in the presence of compliant surfaces such as grassy fields or sandy coasts [2]. Falls and balance-related issues upon stepping from a rigid onto a compliant or uneven surface represent significant threats to the well-being of individuals with LLA and gait impairments, often leading to diminished confidence in mobility and increased risk of injury [3]. As the demographic of people with gait impairments due to amputation or aging continues to grow, the imperative to address the challenges posed by compliant surfaces becomes increasingly pressing. Effective interventions in this context necessitate a comprehensive understanding of the biomechanical intricacies involved in human walking [4].

The role of vision and haptic sense in the process of walking adaptation on different types of surfaces is pivotal in order to meet environmental demands and task goals to ensure an adequate level of functioning and participation in indoor and/or outdoor activities [5]. Typically, the nervous system (NS) acquires environmental information about upcoming surface changes and provides necessary proactive and reactive changes to maintain stability [6]. The ability to anticipate the future state of the walking terrain and integrate this information when preparing motor responses constitutes a demonstration of human intelligence that has not so far been seamlessly infused within the control architecture of current prosthetic or wearable technologies.

The preparation of such motor responses, exhibited in the form of increased early lower-limb muscle activation, has been studied extensively during walking tasks that involve obstacle avoidance, ambulation mode changes, as well as running activities [7, 8, 9, 10]. The prediction of intent to switch between different locomotion modes, including level ground walking, stair ascending/descending, and ramp ascending/descending, has particularly attracted a lot of attention over the years. Researchers have specifically focused on identifying and responding to the user's intent by studying the revealed anticipatory activity in terms of both body mechanics and muscle activations [11], as well as by developing environment-aware approaches [12]. Other relevant works are focused on the integration of sonomyographic and/or electromyographic (EMG) sensing within powered assistive devices to predict user intent and accurately map it to device control parameters [13, 14], while substantial attention has also been given to approaches controlling the powered prosthesis kinematics [15, 16, 17].

Some advancements have also been made in prosthetic foot design towards improving prosthetic adaptability by incorporating variable stiffness mechanisms to allow for more biomimetic and task-specific functionality. Specifically, the Variable-Stiffness Foot (VSF) is a semi-active lower-limb prosthesis that dynamically adjusts forefoot stiffness based on user activity, optimizing energy storage and return while maintaining a lightweight and compact design [18]. Human subject testing with the VSF showed that varying stiffness settings can enhance gait adaptability and user comfort across different walking conditions (e.g., stairs, ramps, and turns). Similarly, the VSPA Foot - a quasi-passive ankle-foot prosthesis with continuously variable stiffness - has been developed to enable transtibial amputees to achieve a more natu-

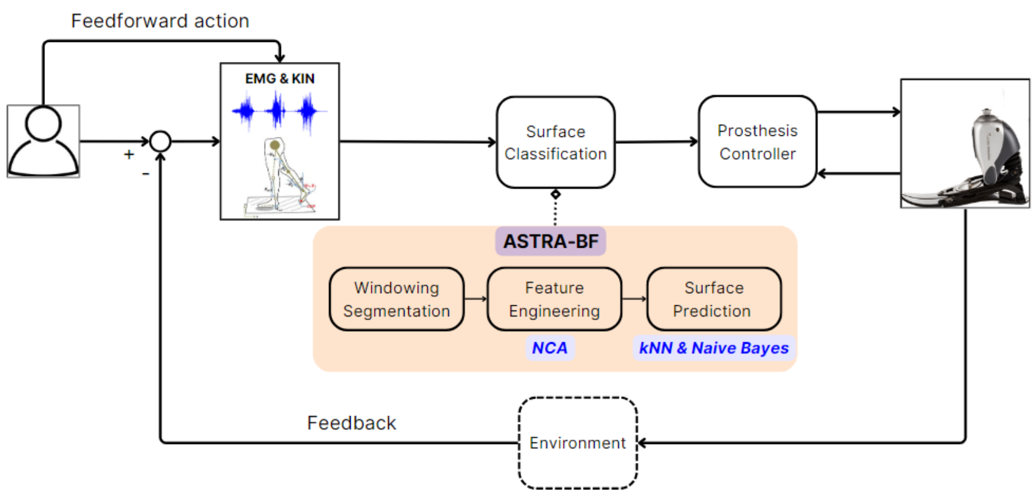

Figure 1: Overview of the proposed research framework and its application on a robotic ankle-foot prosthesis that interacts with the human user and the environment.

ral range of motion during diverse mobility tasks, including stair and ramp ascend [19].

However, despite current progress in the development of user-intuitive prostheses for transitioning between locomotion modes, terrain adaptability of lower-limb prostheses for natural and intuitive walking remains a challenge. The anticipatory mechanisms involved during transitions between dynamic terrains, and especially from rigid to compliant surfaces, have only recently been explored. Relevant works demonstrate significant activity changes in both lower limbs just before an individual encounters a compliant terrain [20, 21, 22, 23]. Leveraging the existence of early muscle contraction during transitions between rigid and compliant terrains, our recent works incorporate distinct user biomechanical signals into an intelligent pattern-recognition control framework that attempts to reproduce NS functionality [24, 25].

The proposed intelligent system features a multi-tiered control framework for robotic ankle-foot prostheses, designed to interact with both the human user and the surrounding environment. This architecture is based on user input with the individual initiating movement through a combination of feedforward (intended movement) and feedback (reaction to the environment) actions. Recorded electromyography (EMG) signals and kinematics (KIN) capture muscle activity and limb movement, revealing the user's intent. This information then flows to a surface classification step, where ASTRA-BF is used to determine the terrain compliance the prosthetic is about to encounter. Based on the predicted surface compliance, the prosthesis controller adjusts the prosthetic limb's behavior before foot contact with the ground, making real-time modifications to suit the terrain. The prosthetic limb then moves according to these adjustments and interacts with the environment. This interaction generates feedback that loops back into the system, allowing it to continuously refine its control decisions. This adaptive control system illustrated in Figure 1 enables the prosthetic limb to dynamically respond to different surfaces, enhancing the user's stability, comfort, and functionality across terrains of varying stiffness.

The goal of our research is to continue to address robust walking over dynamic terrains with different stiffness properties for people with gait impairments and those with LLA. Going beyond our previous works [24, 25], in this paper, we focus on the surface classification module of the proposed controller framework and we present a set of significant advancements, which are encompassed within a novel and efficient Algorithm for Surface TRAnsitions prediction using Biomechanical Features, called ASTRA-BF. Specifically, with ASTRA-BF, we investigate the addition of more than one level of stiffness for the case of compliant terrains, extending the applicability of our work to a range of surfaces found in everyday life. We systematically study the influence of multiple stiffness levels on the anticipatory mechanisms elicited during transitions between rigid and compliant terrains. This work also explores the role of a new set of features used for predicting surface transitions, including autoregressive model coefficients, vertical Ground Reaction Forces (vGRF), as well as Center of Mass (CoM_{xyz}) translation during locomotion. Contrary to our previous works, we also study the effect of the total number of sensors on the classification accuracy, without removing any sources of information (i.e., muscles that might not be available in individuals with LLA), expecting that the feature selection method employed will be able to discern the most beneficial feature variables for the population tested. Our current methodology is differentiated on the basis of the feature selection method, as well as the classification technique used to derive a final decision for the user's next step. Finally, we apply and test the developed framework on both healthy and clinical populations, demonstrating its success on a subject-specific basis.

The capability of robotic prostheses to facilitate transitions on compliant surfaces is essential for daily task performance in individuals with LLA, yet it has not been thoroughly explored in the field. To our knowledge, ASTRA-BF is the first real-time prediction algorithm for soft surface transitions. The results of this study can contribute important knowledge on human anticipatory mechanisms and lead to a new generation of prosthetic and wearable devices that will incorporate the human wearer in the loop and proactively adjust their control to transition to surfaces of different compliance. We expect that instilling this level of human intelligence into prostheses will positively impact the quality of life for people with LLA, empowering participation in many more aspects of daily living.

2. Methods

2.1. Participants

We recruited seven able-bodied (AB) participants (average age: 26.4 ± 1.2 years) free from any orthopedic or neurological pathology that could affect their ability to walk. The AB participant pool consisted of four individuals identifying as male and three individuals identifying as female. Two out of the seven participants (1 male and 1 female) who completed the study were excluded from the analysis as outliers due to noise artifacts as well as inconsistencies during the data collection.

To explore the mechanisms of human locomotion in individuals with LLA, we recruited one participant with a unilateral transtibial amputation (TTA) (age: 47 years, female). The participant was reported to be an active community ambulator, using their prosthesis for at least 12 hours each day. They did not report any nerve damage or sensory issues and did not disclose any comorbidities that could impact their involvement in the study. The cause of amputation was congenital absence of the left ankle and foot. The participant was fitted with a Carbon/Epoxy-Acrylic/ Expandable Patellar Tendon Bearing (PTB) socket attached to an Ossur LP Variflex K3 foot, which was worn by the participant throughout the duration of the study (see Figure 2).

Each participant provided written consent at the time of the experiment after a thorough explanation of the experimental protocol and the nature of the study was provided by the researchers. The experimental protocols for both populations were approved by the University of Delaware Institutional Review Board (IRB ID# 1544521-7 & IRB ID# 1520622-8.).

2.2. Variable Stiffness Treadmill (VST)

The walking assessment of the participants was conducted using a unique robotic platform developed by our lab, the Variable Stiffness Treadmill (VST).

Figure 2: The experiment setup including a view of the VST 2 and the visual feedback monitor. Subject instrumentation is shown, including EMG electrodes and reflective motion capture markers. The image shows the TTA participant walking on the VST 2, preparing to transition to a low stiffness (S_L) surface with their left (prosthetic) leg.

The VST is a split-belt treadmill capable of interactively and dynamically changing its vertical compliance to simulate compliant surface walking scenarios [26, 27].

The first iteration of the VST (VST 1), can specifically alter the stiffness of the left belt within a range of 1 MN/m, which corresponds to rigid ground walking, to about 60 N/m, which corresponds to the highest level of deflection of the walking surface that can be achieved by the VST 1 [27]. The most recent iteration of the VST (VST 2) can dynamically alter the vertical stiffness of both belts within a range of 1.5 MN/m, which corresponds to rigid ground walking, to 13 kN/m, which corresponds to the stiffness of a soft foam mattress [28]. These treadmill settings capture the complexities of everyday walking by recreating compliant surface walking and reproducing in-lab realistic stiffness conditions. The VST 1, which was used to complete experiments with the AB population, was replaced by the VST 2 in completing the experiment with the TTA participant (see Fig. 2) for a variety of reasons pertaining to comfort and accessibility, as well as the safety of

	Max Stiffness Value (kN/m)	**Minimum Stiffness Value** (kN/m)	**Left Belt Deflection** (cm)
R	1000	1000	0
S_H	110	70	1
S_M	69	40	2
S_L	39	20	3

Table 1: Stiffness ranges of each tested condition and their corresponding left belt deflection.

individuals with LLA. The term VST will hereon be used interchangeably to refer to both iterations of the treadmill.

2.3. Experimental Protocol

Before starting with data collection we introduced participants to the VST. The acclimation phase of the study consisted of several minute-long trials, where each subject familiarised themselves with walking over rigid ground (R), as well as three different levels of surface stiffness that were labeled from least to most compliant as High (H), Medium (M), and Low (L) stiffness surfaces. To have consistent stimuli in terms of the walking surface across subjects, we required that the vertical deflection (d) achieved while walking on those three different surfaces be the same across subjects. Therefore, we set the desired vertical belt deflection for H to be approximately $d_H = 1cm$, while for M and L to be $d_L = 2cm$ and $d_L = 3cm$ respectively. Based on this requirement and each participant's weight (b) measured before the trial, a set of desired belt stiffness levels (S) were determined as shown below:

$$S_i = \frac{b}{d_i}, \quad i \in \{H, M, L\} \tag{1}$$

Table 1 shows the belt stiffness ranges for each of the three surfaces, calculated using the weight range of our participants, where S_H, S_M, and S_L correspond to the H, M, and L stiffness surfaces respectively. Those stiffness ranges cover a wide range of real-world ambulation environments, such as balancing on a yoga mat (S_H), walking on grass (S_M), or enjoying a walk on a sandy beach (S_L).

During the acclimation phase, the participants were also able to choose a comfortable walking speed that closely mirrored their typical, everyday walking patterns. We tested different treadmill speeds for each AB participant, concluding at a chosen speed value of 0.90 m/s for all. For the TTA participant, an overground walking test was carried out by a licensed physical therapist (PT) with expertise in LLA evaluation to decide on a suitable treadmill speed. The selected comfortable walking speed for the TTA on our treadmill was 0.7 m/s. It must be noted that the specific properties of our instrumented treadmill platform made the comfortable speed selection lower than what all participants would choose overground, which is expected for this kind of study.

After completion of the acclimation phase, the participants were asked to complete the evaluation trials, during which data collection took place. The evaluation trial protocol was based on the assumption that transitions between surfaces in everyday life activities are first experienced by one leg. Therefore, the right/ intact side of the VST remained rigid for the entire duration of our experiments, while expected stiffness changes were applied unilaterally to the left/ prosthetic side for the AB and TTA participants, respectively. Belt stiffness changes were introduced at regular intervals, specifically every 3 to 5 consecutive rigid gait cycles, and the timing of each stiffness change was coordinated to ensure that during a compliant gait cycle the left/ prosthetic side consistently encountered a walking surface with a S_H, S_M, or S_L stiffness accordingly.

Each participant completed three 5-minute trials. For each of these 5-minute trials, unilateral stiffness changes of only a single condition (S_H, S_M, or S_L) were included. The order of the 5-minute trials was randomized between subjects, while breaks were enforced between trials to eliminate the possibility of artifacts due to subject fatigue. Finally, all participants were required to wear a body weight support (BWS) harness throughout the whole duration of the experiment session. The BWS did not offset any of the subject's weight and was exclusively used for safety purposes.

All stiffness changes were expected, meaning that subjects were notified about an upcoming change in the surface stiffness as early as three steps before it occurred. The participants were provided with a visual cue that was synchronized with their gait. With every completed gait cycle, a colored patch (green for H, yellow for M, red for L, and blue for R) would move from the top toward the bottom of a screen that was placed in front of the treadmill. The bottom of the screen corresponded to the participant's current step, so whenever the colored patch reached the bottom, the subjects knew that the upcoming step would take place on compliant ground, as well as the level of stiffness they would encounter (see Figure 3).

2.4. Data Collection

During all trials and sessions, we collected EMG signals from several muscles of the left and right limbs. EMG wireless sensors (Trigno, Delsys Inc.) were specifically placed on the following muscles of both limbs: tibialis anterior (TA), soleus (SOL), gastrocnemius (GA), rectus femoris (RF), vastus medialis (VM), vastus lateralis (VL), and biceps femoris (BF). Muscle selection was guided by their primary functions in ankle motion and stability [29]. The EMG signals were sampled at 2 kHz. The data recorded were separated between muscle activations from the left (L) and the (R) leg. Therefore, the notation we will follow in this paper will include an L or an R ahead of the muscle name (i.e., LTA for the TA of the left leg) to indicate which leg we are referring to. The location of the muscles was determined via anatomical landmarks of the limb, following SENIAM recommendations [30]. It should be noted that for the TTA participant the LTA, LSOL, and LGA muscle activities were not recorded, due to the inability to place the EMG electrodes within the prosthetic socket.

Additionally, we recorded vGRFs using high-resolution force mats (Tekscan 3510 Medical Sensors for VST 1 and TekScan 3140 with VersaTek Cuffs for VST 2) inserted between the belts and the treadmill supporting platform. These mats collect force data with a spatial resolution of 1 cm in both the anterior/ posterior and medial/ lateral directions. There are 4224 force-sensing cells on each treadmill belt. The total force applied was then determined by summing the measurements from all the force cells. Force data were collected at a frequency of 65 Hz.

We also collected lower-body kinematics using 20 reflective markers on the pelvis, thighs, shanks, and feet of the subjects. Markers were located according to Vicon's Plug-in Gait Lower-body model [31], and data was sampled at 100 Hz using a Vicon motion capture system integrated with the VST implementations.

2.5. Data Processing

Throughout the data processing pipeline, particular emphasis was placed on noise reduction and the robustness of the employed methodologies. Specifically, we employed robust filtering techniques to minimize high-frequency

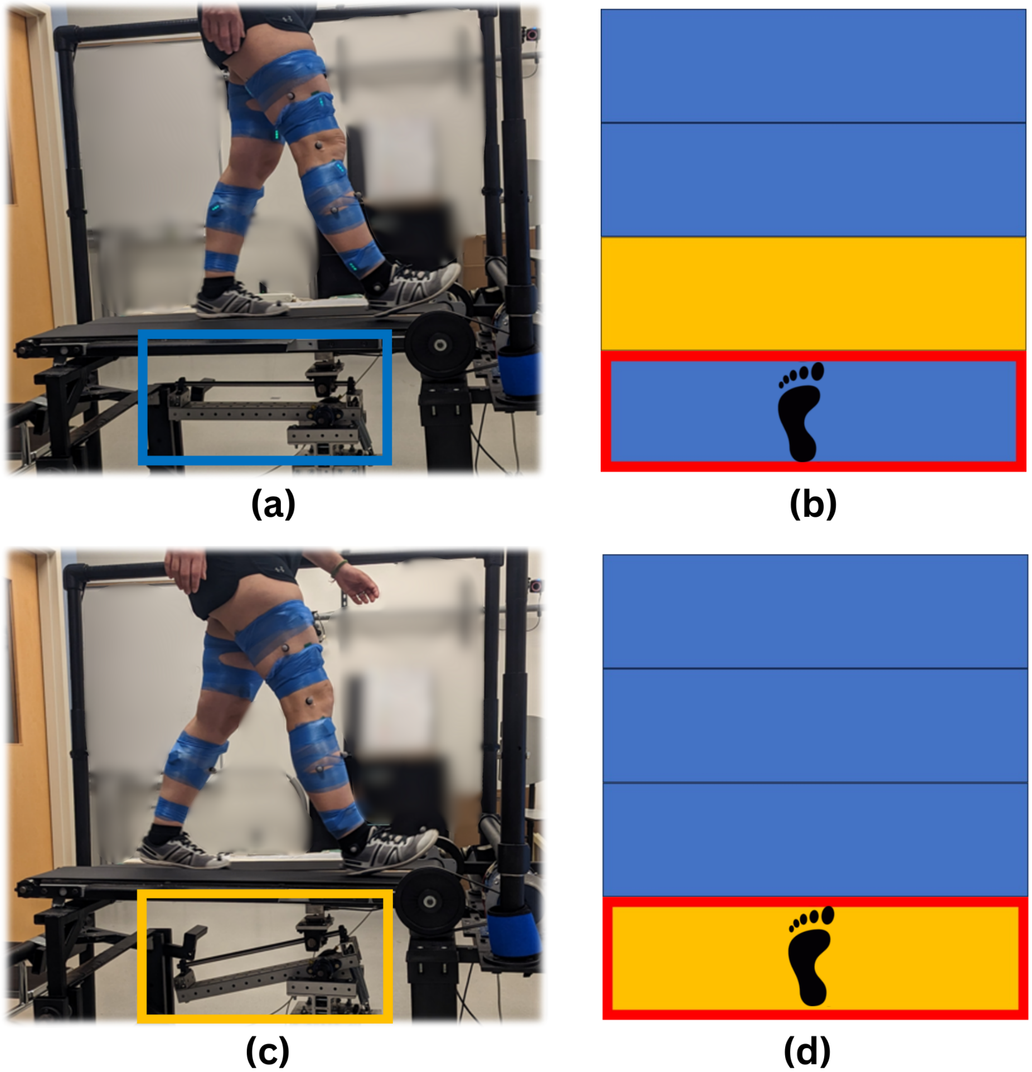

Figure 3: Visual feedback setup during walking trials on the VST 1. (a) AB subject transitioning from a rigid to another rigid surface. Both VST 1 belts are set to rigid. (b) Visual feedback seen by the subject during the experiment. Blue corresponds to rigid (R) ground walking. The red rectangle denotes the user's current step. (c) AB subject transitioning from a rigid to a medium compliance (M) surface. The right VST 1 belt is set to rigid, while the left belt is set to compliant (M). The left VST 1 belt deflects. (d) Visual feedback seen by the subject during the experiment. Yellow corresponds to M compliant ground walking.

noise and movement artifacts, and used feature normalization to reduce variability caused by individual differences. These precautions were taken in an effort to minimize uncertainty and maximize the robustness of the proposed framework.

Utilizing a robust kinematic algorithm for heel-strike detection [32], we synchronized the raw kinematic and EMG data and segmented the trials into distinct gait cycles following the convention that each gait cycle begins and ends at Left Heel Strike (LHS). Force mat data were also synchronized with motion capture and EMG data using a trigger signal from Vicon Nexus. Then, for each subject, outlier gait cycles were detected using a systematic method [33] that analyzed kinematic data in all three directions at the hip, knee, and ankle, as well as muscle activity data for all reported muscles. This systematic outlier detection ensured that noisy or irregular gait cycles, which could adversely affect downstream analyses, were excluded, thereby enhancing the robustness of the employed algorithmic implementation against noise and uncertainty. As outlined above, the acclimation phase was excluded from the data analysis and will not be discussed further.

For each subject and muscle, the raw data sampled at 2 kHz were first filtered with a fourth-order Butterworth band-pass filter, with a low and high cut-off frequency of 30 Hz and 300 Hz, respectively. As a next step, the data underwent full-wave rectification, and the linear envelope of the muscle signal was computed by using a moving average with a window size of 200 data points. Data was subsequently subjected to an additional fourth-order Butterworth low-pass filter with a cut-off frequency of 4 Hz. To standardize the EMG data, the final processed values were normalized based on the maximum muscle activity observed during the experiment. Finally, the EMG data were downsampled to 100 Hz using linear interpolation to match the frequency of the motion capture data. This process produced useful muscle activity data scaled at a range of 0%–100% activity level.

2.6. Data Analysis of Expected Stiffness Changes

The study focuses on studying the anticipatory mechanisms involved in human locomotion before encountering a compliant surface. Therefore, the data analysis concentrates on the gait cycle preceding each stiffness change. The gait cycles of interest were specifically labeled as i) transition to high (TH), ii) transition to medium (TM), and iii) transition to low-stiffness (TL) surface if the participant was preparing to step on a S_H, S_M, or S_L surface respectively. All transitions were initiated on rigid ground to ensure uniformity across the different conditions. The rigid gait cycles were labeled as R, while it should be noted that the R gait cycles immediately following a stiffness change were excluded from the data analysis to eliminate any possible aftereffects.

2.7. Windowing Segmentation Analysis

Windowing techniques enable data analysts to identify valuable patterns in time-series data. Sliding windows are particularly powerful because they allow us to spot patterns earlier than other techniques [34]. This feature becomes crucial in scenarios where the ability to make a critical decision in real-time, such as in our case, is important. More specifically, detecting the surface transition in real-time before stepping on it is vital in our proposed system for preventing balance-related falls in TTA populations.

Our approach includes a continuous sliding window technique that divides the EMG and kinematic signals of every gait cycle into 150 ms long windows [35]. A 50% window overlap was selected for continuous feature extraction. To ensure intrasubject uniformity and cohesion between the different gait cycles, the EMG and kinematic data were resampled to the average number of samples observed within each subject before proceeding with the windowing segmentation. Our focus is concentrated between the terminal stance (before left toe-off (LTO)) and swing phase (before LHS) of each gait cycle, rather than the whole duration of a gait cycle. This tactic is in line with our hypothesis that the prediction accuracy of the classifier will be higher toward the end of each gait cycle, as the subjects approach a compliant surface, and is also supported by our previous work [23]. In total, the result of the segmentation was six sliding windows, which were analyzed both as single entities and cumulatively to assess their predictive influence on the user's intent to step on a compliant surface. All data was segmented into sliding windows, with the sole exception of the GRF data of each gait cycle, as the availability of the GRF data is specifically restricted to the stance phase of the left foot (LHS to LTO) while the foot still maintains contact with the force mat.

2.8. Feature Engineering for Gait Classification and Prediction

In the context of gait classification, a prevailing methodology involves the integration of data sourced from an array of sensors to enhance confidence in decision-making as compared to reliance on individual sensors. A customary approach to data integration in this regard is pattern-level fusion [36]. In this paradigm of data fusion, distinct feature vectors are initially derived from signals captured by each sensor, and subsequently, these feature vectors are concatenated to form a unified feature vector. Concatenating feature vectors obtained from various sensors naturally leads to the increase of the dimensionality of the resultant feature vector, which is deemed undesirable due to concerns related to both efficacy and efficiency. Consequently, a pivotal preprocessing step in the implementation of gait classification involves the reduction of feature vector dimensions before deployment for classifier training. Ultimately, our goal is to identify the feature subset that yields the most accurate results with the least amount of sensor data that can be used.

Two primary categories of algorithms are instrumental in achieving dimensionality reduction: 1) feature extraction and 2) feature selection. Specifically, feature extraction involves the derivation of the ultimate feature set through the combination of initial features, while feature selection entails the identification of a subset from the original set of features.

2.8.1. Feature Extraction in the Time-Domain (TD)

Time-domain (TD) features, acknowledged for their swift time response in real-time settings, are widely employed in pattern recognition, a quality that makes them particularly suitable for integration within this framework.

As an extension to our previous work [24], we augmented the number of extracted features to include i) new features, such as the autoregressive (AR) model coefficients [37] and the GRF values, as well as ii) increased the number of signal sources included in the analysis. For this work, no muscles were excluded from the feature engineering investigation to unbiasedly assess the influence of each variable on the final prediction and evaluate which signal sources were selected by our framework. In total, a set of 18 EMG [24], and 3 KIN features were extracted per signal source (refer to Table 2). This extraction process yielded an EMG feature vector $\boldsymbol{f_{EMG}}$, as well as a KIN feature vector $\boldsymbol{f_{KIN}}$ per segmented window. The size of the feature vectors varied between the AB and TTA participants since some muscles (LTA, LGA, and LSOL) were not available for the latter case. The result of the feature extraction was, therefore, a horizontally concatenated feature vector $\boldsymbol{f}$ of 303 and 249 features per window for the AB and TTA participants, respectively.

As previously mentioned, due to the nature of the GRF curve, we isolated the stance phase of each gait cycle to extract 3 stand-alone characteristic sig-

	Signal Source	Extracted Features
EMG	TA, SOL, GA, RF, VM, VL, BF	Mean Absolute Value
		Waveform Length
		Difference Variance Value
		Root Mean Square
		Simple Square Integrated
		Integrated EMG
		Variance of EMG
		Difference Absolute Mean Value
		Standard Deviation
		Average Amplitude Change
		Kurtosis
		Skewness
		6th order AR coefficients [37]
KIN	Ankle/ Knee/ Hip Flexion, Ankle/ Knee Vel. & Acc, Center of Mass (CoM_{xyz})	Maximum value
		Minimum value
		Mean value
GRF	Left Force Mat	1st peak
		2nd peak
		Minimum valley point

Table 2: Set of TD features chosen to be extracted from the EMG and kinematic (KIN) signals. The EMG signal sources refer to the muscles of both limbs that were included in the analysis. The KIN signal sources refer to the x, y, and z center of mass coordinates, the joint properties of the ankle, knee, and hip of both limbs (17 signal sources), as well as the force mat GRF data during the stance phase of the left leg (1 signal source). The extracted features include the type of information that was drawn from each signal source per segmented window.

nal features as described in Table 2. The GRF features were extracted after careful observation of the vertical GRF curve, which specifically consists of two peaks: the passive (1st) peak, corresponding to weight acceptance, and the active (2nd) peak, corresponding to push-off [38]. In between these peaks, as the subject weight is distributed from heel to toe, a valley area is formed, the minimum of which corresponds to the third GRF feature extracted. The resultant feature vector thus takes the form: $\boldsymbol{f_{GRF}}= [f_{1stpeak}, f_{2ndpeak}, f_{valley}]$. The extracted GRF features were then temporally and horizontally concatenated to the feature vector created for each of the segmented windows, resulting in a final feature vector of 306 or 252 features ($\boldsymbol{F}$) per segmented window

q for the case of the AB and TTA participants respectively, as shown below:

$$\boldsymbol{F_q} = [\boldsymbol{f}, \boldsymbol{f_{GRF}}]_{\boldsymbol{q}} \tag{2}$$

2.8.2. Feature Selection using Neighborhood Component Analysis (NCA)

Neighborhood Component Analysis (NCA) is a non-parametric method for selecting features to maximize the prediction accuracy of regression and classification algorithms [39]. For the current study, we performed NCA feature selection to learn the feature weights for the minimization of an objective function that measures the average leave-one-out classification loss over the training data [40]. NCA specifically works by assigning a feature weight (FW) to each predictor to indicate its relevance to the classification process. Higher weights denote greater importance, while weights approaching zero signify redundant features. The weight threshold (θ_w) was set as $\theta_w = T \cdot max(FW)$, where $T = 0.4$. More information about the NCA implementation, as well as the specific contributions of the selected features, have been further analyzed in our previous work [40].

Among other advantages, NCA preserves the interpretability of features by selectively choosing a subset from the initial feature set to accomplish dimensionality reduction. Notably, NCA possesses the capability to leverage the available class label information throughout the reduction process. The integration of class information by NCA is executed in a manner that renders the data, post-reduction in dimensionality, amenable to gait prediction classification. The NCA algorithm implementation was completed using the $fscnca$ Matlab command, which uses the regularized objective function [39].

2.9. Gait Prediction and Classification

The formulation of the classification problem at hand pertains to multiclass classification, including surfaces of variable stiffness, ranging from high to low-stiffness terrains. This multiclass setup requires the model to differentiate between multiple classes rather than a simple binary distinction, adding complexity to the prediction task. Accurate classification within this multiclass framework allows the prosthesis controller to make precise, real-time adjustments, optimizing the user's stability and comfort across diverse environments.

2.9.1. Data Balancing

A critical step before classifying the available data is ensuring that the classification input is free of biases that might affect the final prediction results. Adhering to the 70/30 rule, we divided the selected feature data into the *training* and *testing* sets. Due to the structure of the experimental protocol, the R cases significantly outnumbered the compliant surface cases (TH, TM, TL), leading to an imbalanced classification problem. To mitigate the impact of the data imbalance, we implemented the Synthetic Minority Oversampling TEchnique (SMOTE) in our training set [41, 42]. SMOTE accomplishes the oversampling of the minority class through the creation of "synthetic" examples, diverging from conventional oversampling with replacement. In this process, synthetic instances are introduced along line segments that connect any or all of the k' nearest neighbors belonging to the minority class. The selection of neighbors from the k' nearest neighbors is randomized and contingent on the targeted degree of oversampling; in our specific implementation, we employed $k' = 5$ nearest neighbors. Additionally, a random undersampling of the R cases was applied in the test set.

2.9.2. k Nearest Neighbors (kNN) Algorithm

The potential of the kNN classification algorithm to produce reliable and accurate predictions of user intent to transition to a compliant surface has already been demonstrated in previous works [24, 25] and is therefore selected as the primary classification method for the current study. In particular, the simplicity of the algorithm stands out as a notable feature. By employing straightforward comparisons to identify similar records in the training data, the kNN algorithm demonstrates effectiveness in generating accurate predictions. Furthermore, kNN proves effective in capturing intricate interactions among variables without necessitating the definition of a separable statistical model, thus eliminating the need for coefficients and weights. Additionally, kNN comes with the advantage of not imposing any assumptions on the data, which differentiates it from certain other algorithms. For instance, Multiple Linear Regression (MLR) tends to perform optimally when the data exhibits normal distribution and when the relationships between predictors and outcome variables are approximately linear. In contrast, kNN can perform effectively without mandating the fulfillment of such assumptions.

For this implementation, our approach involved employing an Euclidean distance metric between a test and a training data point, accompanied by an inverse distance weight. The rationale behind employing an inverse distance metric is to reduce the influence of noisy far-off points by assigning higher weights to closer neighbors in the distance metric. The selected number of neighbors was defined as $k = 9$ after relevant investigation and result cross-validation for assessing model performance under various conditions and optimizing hyperparameters, thus maximizing prediction accuracy. Each predictor variable underwent centering and scaling based on the corresponding weighted column mean and standard deviation. A distinct classifier was trained for each segmented window, resulting in a total of six separate classifiers and decisions per gait cycle.

2.9.3. Naive Bayes Classification

The aforementioned method for feature selection and classification resulted in classification decisions for each of the six windows. To reach a final decision about the user's next step, we need to combine the distinct classifier decisions into a conclusion about the stiffness of the upcoming surface. To achieve that we employed a Naive Bayes classifier, which combined the six individual decisions of the kNN window classifiers into a final decision.

Naive Bayes classification is a probabilistic machine learning algorithm rooted in Bayesian probability theory. It operates on the assumption of feature independence, given the class label, hence the term "naive." The algorithm calculates the probability of a data point belonging to a particular class based on the probabilities of its individual features given that class [43]. Naive Bayes classifiers assign observations to the most probable class, which corresponds to the maximum a posteriori decision rule. Explicitly, the algorithm estimates the densities of the predictors within each class and models the posterior probabilities according to the Bayes rule for all $n = 1, ..., N$, as:

$$\hat{P}\left(Y = n | X_1, \ldots, X_q\right) = \frac{\pi(Y = n) \prod_{j=1}^{q} P(X_j \,|\, Y = n)}{\sum_{n=1}^{N} \pi(Y = n) \prod_{j=1}^{q} P(X_j \,|\, Y = n)} \tag{3}$$

, where Y is the random variable corresponding to the class index of an observation, $X_1, \ldots, X_q$ are the random predictors of an observation, and $\pi(Y = n)$ is the prior probability that a class index is n.

In the context of our surface classification problem, we can relate the components of the Naive Bayes classifier to our specific application, where Y represents the surface stiffness we aim to predict, such as R, S_H, S_M, or S_L, making this a multiclass classification problem. Each class is indexed by n, which corresponds to the respective stiffness level (e.g. n=1 for R, n=2 for S_H, n=3 for S_M, and n=4 for S_L). The predictors $X_1, \ldots, X_q$ are the decisions derived from each segmented window q, capturing different aspects of the user's gait cycle that correlate with specific terrains. Finally, the prior probability $\pi(Y = n)$ represents the likelihood of encountering a specific level of surface stiffness, which is set to 0.25, as we consider the four different terrains equally likely to happen.

Naive Bayes classifiers are relatively quick to train, which is beneficial for real-time applications and is also one of the reasons we opted for this approach. Specifically, utilizing the trained window kNN classifiers, we leveraged the available training data to derive a decision (R, TH, TM, or TL) for each window within every gait cycle. Subsequently, these decisions were incorporated into the training process of the Naive Bayes, while the testing data originally employed for assessing the kNN classifiers were repurposed for the evaluation of the Naive Bayes performance as well. Utilizing the independent window decisions that resulted from the kNN classification, we serially implement the Naive Bayes using the decisions from Windows 1, then the decisions from Windows 1 and 2, from Windows 1,2, and 3, and so on until all window decisions are included. The goal of this approach is to evaluate how early within the windowing process we can derive a final decision about the upcoming surface stiffness.

The incorporation of the Naive Bayes into our research strategy is geared toward crafting a resilient, precise, and expeditious real-time user intent recognition framework. Real-time classification demands a decision to be reached before LHS, preceding the transition onto the new surface—be it rigid or compliant. Our hypothesis posits that a serial combination of distinct classifier decisions will enhance overall accuracy and expedite prediction times.

2.10. Classification Performance Assessment

The most instrumental metrics in assessing the effectiveness of the ASTRA-BF control framework include the Balanced Accuracy and the Macro F1-Score [44]. These metrics are derived from the Confusion Matrix, which encloses all the relevant information about the algorithm and classification rule performance. The notation that is used in the following equations refers to the true positive (TP), false positive (FP), true negative (TN), and false negative (FN) elements of the confusion matrix as defined for multiclass classification.

2.10.1. Balanced Accuracy

The Balanced Accuracy (α) formula essentially computes an average of recalls. Initially, we assess the Recall (r) for each class, and subsequently, we average these values to derive the Balanced Accuracy score. The Recall value for each class addresses the question of how likely an individual of that class will be correctly classified. Therefore, the Balanced Accuracy offers an averaged representation of this concept across different classes, and is defined below:

$$\alpha = \frac{r_R + r_{TH} + r_{TM} + r_{TL}}{4} \tag{4}$$

In scenarios where the dataset is well-balanced, indicating that the classes are nearly of the same size, both Accuracy and Balanced Accuracy tend to converge towards the same value. The primary distinction between Balanced Accuracy and Accuracy becomes apparent when the initial dataset, i.e., the actual classification, exhibits an unbalanced distribution among the classes. Balanced Accuracy is therefore preferred over simple Accuracy as it is insensitive to imbalanced class distribution, and it gives more weight to the instances coming from minority classes.

2.10.2. Macro F1-Score

In the context of multi-class scenarios, the calculation of the F1-Score ($f1$) necessitates the inclusion of all classes. This involves incorporating multi-class measures of Precision and Recall into the harmonic mean. To specifically compute the Macro F1-Score, it is essential to first calculate Macro-Precision and Macro-Recall. Macro-Precision is determined by averaging the precision values for each predicted class, while Macro-Recall involves averaging the recall values for each actual class. The Macro approach treats all classes as fundamental elements in the calculation, assigning equal weight to each class in the average. Consequently, there is no differentiation between highly and poorly populated classes in this approach.

Precision (p) and Recall (r) for each class are calculated using the same formulas as in the binary setting, which are also provided below for a generic class $c = R, TH, TM, TL$.

$$p_c = \frac{TP_c}{TP_c + FP_c} \tag{5}$$

$$r_c = \frac{TP_c}{TP_c + FN_c} \tag{6}$$

Macro-Average Precision (μ) and Recall (ν) are then computed as the arithmetic mean of the metrics for single classes, while Macro F1-Score constitutes the harmonic mean of Macro-Precision and Macro-Recall as follows:

$$f1 = 2\frac{\mu \cdot \nu}{\mu + \nu} \tag{7}$$

There is no dependence on class size, as classes of varying sizes are equally weighted in the numerator. Consequently, the impact of larger classes is considered as important as that of smaller ones. The resulting metric evaluates the algorithm from a class perspective: high Macro-F1 values signify that the algorithm performs well across all classes, while low Macro-F1 values indicate poor predictions for certain classes.

2.10.3. Classification Loss

The classification loss also constitutes a helpful indicator representing the predictive inaccuracy of classification models [44]. The classification loss is specifically obtained by the cross-validated classification model. For every fold, we compute the classification loss for validation-fold observations using a classifier trained on training-fold observations. For our case, we calculate the minimal expected misclassification cost by utilizing the resulting posterior probabilities from the kNN implementation. The weighted average of the minimal expected misclassification cost loss for observations $j = 1, ..., n$, is:

$$L = \sum_{j=1}^{n} w_j u_j. \tag{8}$$

, where u_j is the cost incurred for making the prediction and w_j is the weight for observation j. Matlab normalizes the observation weights so that they sum to the corresponding prior class probability stored in the *Prior* property of the kNN classification model. Therefore, $\sum_{j=1}^{n} w_j = 1$. A lower loss generally indicates a better predictive model.

3. Results

3.1. NCA reduced the number of the selected classification input features by 91%

By employing NCA as our feature selection method, we were able to reduce the number of the selected classification input features by 91% on average. To be more specific, the initial 306 (AB) or 252 (TTA) features per window were dropped to approximately 25 ± 5. The variability in the number of selected features stems from the fact that each window corresponds to a distinct classifier, while an inherent variability among subject features is also anticipated. This feature reduction holds significance because the selection of a subset of features plays a crucial role in diminishing the channels of information utilized per experiment, enhancing computational efficiency, and streamlining the classification process.

Examining the frequency of feature appearance across windows and subjects can yield valuable insights about the information channels necessary to develop a robust and reliable high-level control framework for powered prostheses and wearable devices. Figure 4 presents the appearance frequency of the different EMG signal sources (muscles) per window across subjects, while Figure 5 does the same for the kinematic and kinetic signal sources (see Table 2). For example, the LGA muscle covers more area when compared to the LTA muscle for the case of the AB participants, indicating an increased selection of features from that particular signal source and, consequently, its increased importance in the ASTRA-BF prediction framework.

3.2. Thigh muscle features lead the high prediction accuracy

Analyzing the information presented in Figure 4 and Figure 5, we can deduce some important conclusions about the significance of different signal sources in the intent prediction task. Observing the shaded areas of the radar plots, we can see that the most prominently selected signal sources tend to cover a larger area. For the case of the EMG features, LGA, and RSOL as below-knee muscles, as well as LVL, LBF, and RRF as above-knee muscles, form the top 5 muscle signal sources that NCA selects to achieve the highest prediction accuracy for the case of the AB participants. Focusing on the TTA participant results, we observe a similar pattern with the thigh muscle features leading the high prediction accuracy of our framework. Specifically, the RRF, RVM, RBF, and LVL constitute the top 4 above-knee muscle signal sources that NCA selects, with the RGA following as a below-knee muscle.

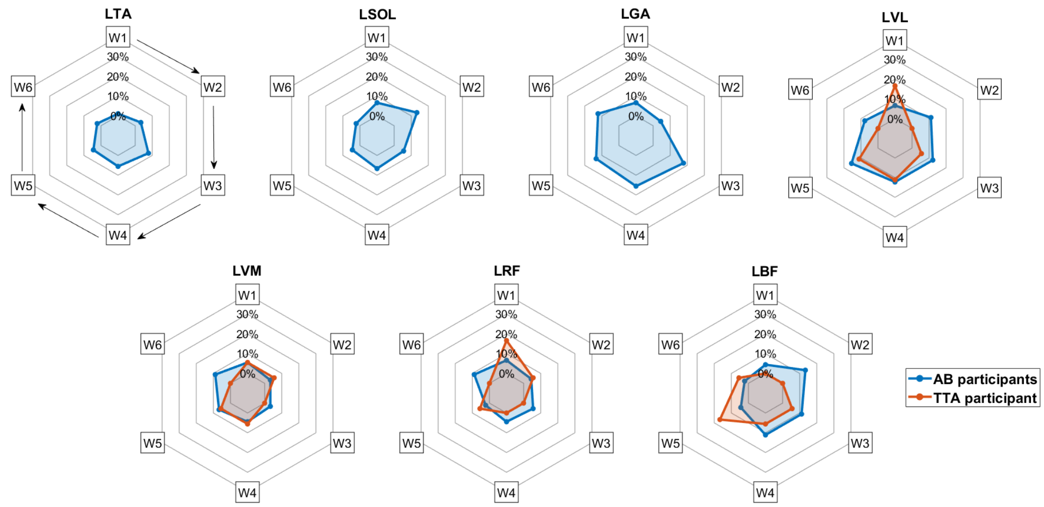

(a) Appearance frequency of the EMG features selected by NCA per muscle for the left/ prosthetic leg.

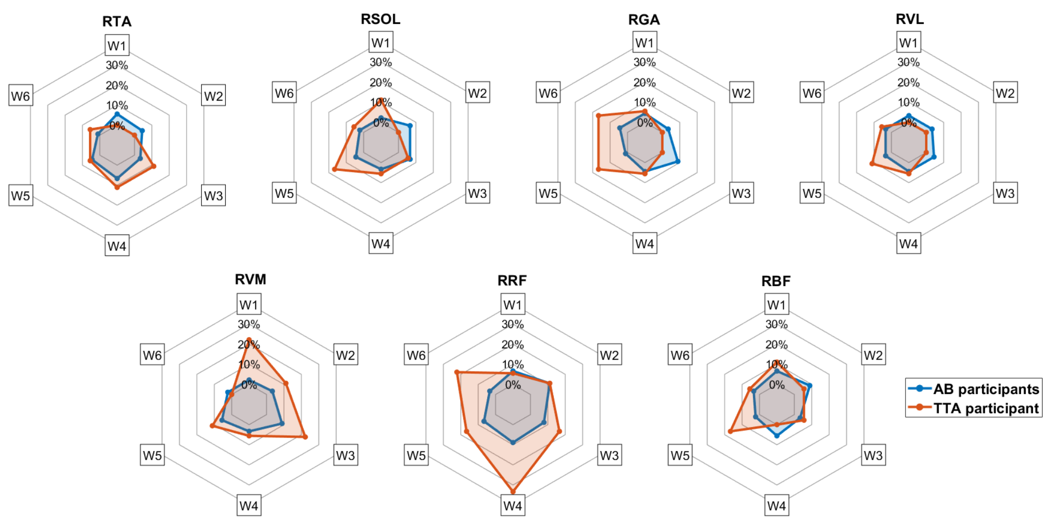

(b) Appearance frequency of the EMG features selected by NCA per muscle for the right/ intact leg.

Figure 4: Radar chart representing the appearance frequency of the selected EMG features per muscle variable. Each muscle has its own plot, while each segmented window (W1, W2, ..., W6) has its own axis, with all axes joining together in the center of the figure. The arrows indicate the order of the segmented windows, starting from W1 (around LTO) through W6 (before LHS). The selection frequency of each feature is expressed as a percent, with larger shaded areas per muscle indicating a more frequent selection of features from that signal source. AB results are expressed as average values across participants per window, while TTA results pertain to a single participant.

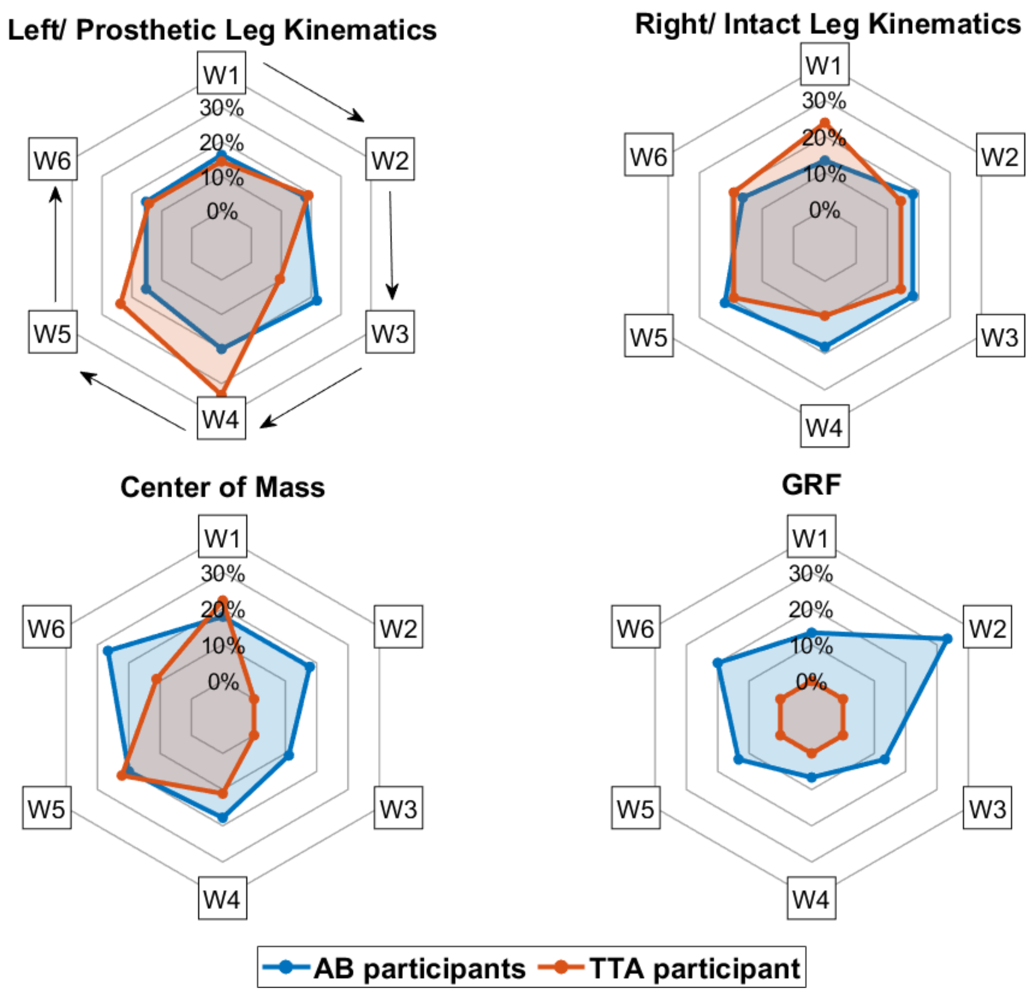

Figure 5: Radar chart representing the appearance frequency of the selected kinematic and kinetic features per signal source. The kinematics (flexion, angular velocity, and acceleration) of the left/ prosthetic leg (ankle, knee, hip) were grouped together (upper left figure) in the same way that the kinematics of the right/ intact leg were also grouped together (upper right figure). Each signal source (left/ prosthetic limb, right/ intact limb, CoM, and GRF) has its own plot, while each segmented window (W1, W2, ..., W6) has its own axis, with all axes joining together in the center of the figure. The arrows indicate the order of the segmented windows, starting from W1 (around LTO) through W6 (before LHS). The selection frequency of each feature is expressed as a percent, with larger shaded areas indicating a more frequent selection of features from that signal source. AB results are expressed as average values across participants per window, while TTA results pertain to a single participant.

These constitute important findings that reinforce and align with the role of hip extensors and hip flexors as major power generators in the absence of ankle plantar flexor power. Notably, in persons lacking ankle plantar flexor power, such as in people with TTA, studies have demonstrated that hip extensors, hip flexors, and hip external rotators play pivotal roles as major power generators [45]. Prior studies have also shown compensations in these muscles, including longer durations of activity in the amputated leg hip extensors and intact leg knee extensors [46].

For the case of the KIN features across the AB participants, right and left ankle accelerations, right knee acceleration, left ankle flexion, and CoM_y form the top 5 kinematic signal sources that NCA selects to achieve the highest prediction accuracy. Similarly, for the TTA participant, right and left knee accelerations, left knee angular velocity, right hip flexion, and right ankle acceleration form the top 5 NCA-selected kinematic signal sources. Ankle and knee acceleration features may suggest an adjustment in step length as participants prepare to step onto a new surface, while ankle angle features could be associated with increased toe clearance during these transitions. Collectively, the selected kinematic features indicate that the non-leading leg can also offer significant insights into user intent when transitioning between compliant surfaces.

3.3. Classification accuracy of ASTRA-BF increases as the participants approach the new surface

The performance of each window classifier confirms that prediction accuracy tends to be higher toward the end of each gait cycle, particularly as we approach the last segmented windows. The evaluation of our best AB subject's performance demonstrates a steady increase in Balanced Accuracy from 45.25% in Window 1 to 82% in Window 6 (see Fig. 6). Notably, the Macro F1-Score also exhibits a similar upward trend toward the final segmented windows, closely following the pattern of the accuracy metric, while the declining trend of the classification loss is correlated with a gradually improving classifier accuracy.

This trend was further validated for all AB participants by studying the average subject performance for each window classifier, as illustrated in Figure 7. The mean subject values for the Balanced Accuracy and Macro F1 metrics exhibit an ascending trend with increasing window numbers, reaching 72.67% and 71.6% in the last segmented window, respectively. Similarly,

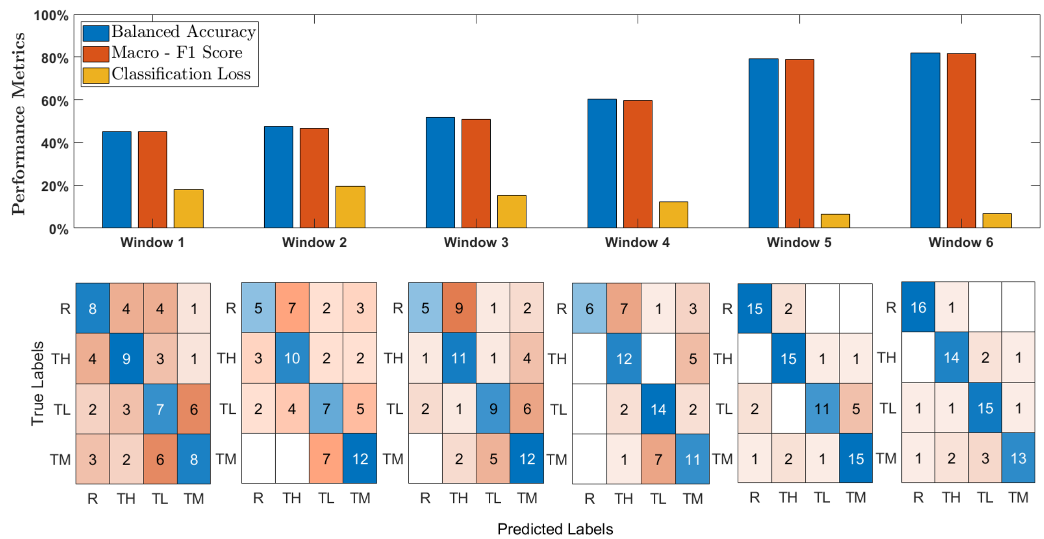

Figure 6: Performance evaluation metrics and corresponding confusion matrices for the best AB subject included in this analysis using k-NN window classifiers.

	Window 1		Window 2		Window 3		Window 4		Window 5		Window 6	
Metric	*Macro*	*Micro*	*Macro*	*Micro*	*Macro*	*Micro*	*Macro*	*Micro*	*Macro*	*Micro*	*Macro*	*Micro*
Precision	0.7516	-	0.70063	-	0.73197	-	0.77652	-	0.77687	-	0.72738	-
Recall	0.74405	-	0.69286	-	0.70595	-	0.76071	-	0.7619	-	0.70952	-
F1-Score	0.73759	0.74138	0.69564	0.68966	0.71419	0.7069	0.75685	0.75862	0.76178	0.75862	0.71215	0.7069

Table 3: Macro and micro metrics for k-NN performance evaluation. In multi-class classification scenarios where each observation is assigned a single label, the micro-F1, micro-precision, and micro-recall metrics will yield identical values. This equivalence explains why we report only the micro F1-score value.

the classification loss for the same window is at 12.83%, demonstrating the classifier's relatively good generalization ability to a new set of data.

For the participant with TTA, we observe a similar trend, which reveals a rise in the Balanced Accuracy metric during windows 4 and 5, achieving a peak accuracy of 76.2% (see Figure 7), which closely follows the average prediction accuracy in the AB participants. A comparable behavior is observed in the Macro F1-Score, Precision, and Recall metrics, which exhibit a similar trend to the accuracy metric (see Table 3).

Additionally, the kNN classifiers of our framework seem to successfully discern between surfaces of very different stiffness (e.g., between rigid (R) and low stiffness surface transitions (TL)). However, we observed that for cases such as rigid (R) and high-stiffness surface transitions (TH) or between

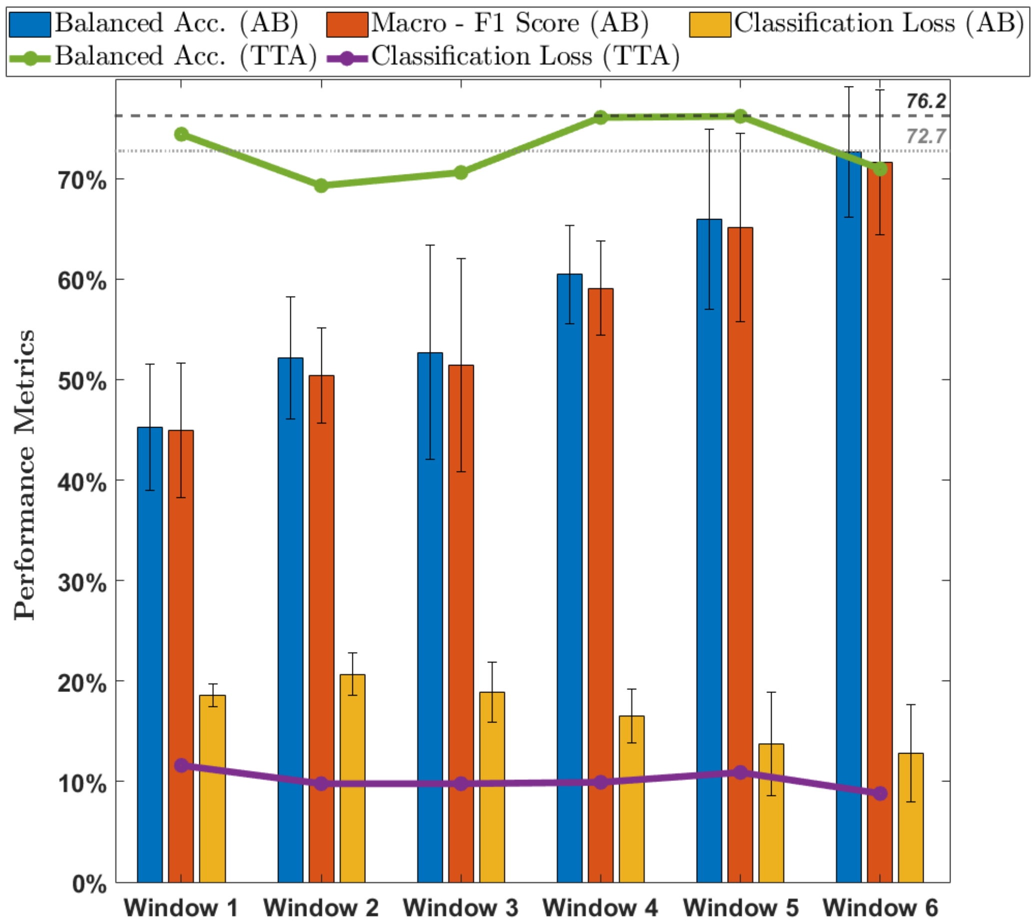

Figure 7: AB and TTA subject average performance evaluation metrics using k-NN window classifiers.

medium (TM) and low-stiffness (TL) surface transitions, our classifiers were more prone to erroneous predictions (see confusion matrices in Fig. 6). We attribute this behavior to the close resemblance of these surface stiffnesses, which increases the difficulty of the classification.

3.4. Reliable predictions were achieved between 75ms-150 ms before stepping onto a new surface

The success of this framework lies within its ability to predict the transitions between surfaces of variable stiffness before they happen, i.e., before the foot of the user lands on the new surface. Based on the AB results shown in Figure 6, we can see that a prediction as early as Window 5 is accurate enough (79.13%) to make a correct decision for the upcoming surface. On average, the same observation is valid across all the subjects that were included in this analysis (see Figure 7), since the Balanced Accuracy and Macro F1-score achieved for Window 5 across all subjects did not present any statistically significant differences with the equivalent metrics for Window 6. For the participant with TTA (see Figure 7), results also show that a prediction decision as early as Window 4 offers a decently accurate prediction (76.2%) about the user's next step.

Since the duration of the overlapping segmented windows is set to 150ms with a 50% overlap, it means that ASTRA-BF can currently make an accurate prediction of the upcoming surface between 75 ms and 150 ms before the user steps on it. Upon making the final decision, the prosthesis's control parameters can be altered to safely accommodate soft surface transitions. An example of a possible control action for a prosthesis is its adjustment of impedance, as shown in our previous work [47]. Given the current computational power of micro-controllers usually found in lower limb prostheses as well as current designs that allow high-frequency control, we believe that this time is enough to alter the prosthesis's control parameters to safely accommodate those transitions.

3.5. Naive Bayes classifier improved the subject average prediction accuracy

Classification results per segmented window result in very promising predictions, reaching an accuracy of 82% for our best AB participant and 76.2% for the participant with TTA. However, to reach a final decision about the user's next step, we need to combine the distinct classifier decisions into a conclusion about the stiffness of the upcoming surface. The addition of the Naive Bayes classification as a cumulative last step to our framework was able to increase the classification accuracy by 4.58% and 6.8% for the AB and TTA cases respectively, when all six windows were included in the framework and by 7.82% and 4.8%, when the first five windows were included, providing us with an early decision of at least 75ms before the actual transition to the new surface (see Figure 8). For comparison purposes, simple and weighted majority vote techniques were also tested against the Naive Bayes approach, resulting in comparable, yet not better, results (Figure 8). As expected, utilizing the weighted alternative of the simple majority vote yielded improved, but not statistically significant, predictions.

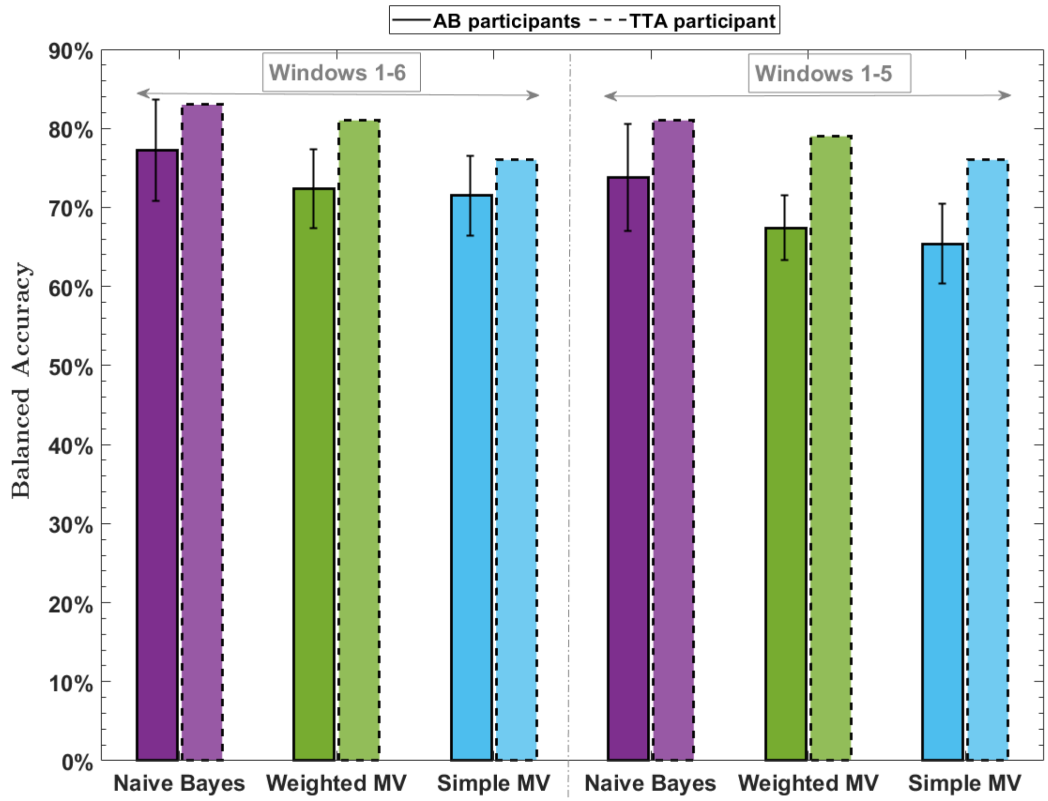

Figure 8: Comparison of the subject average performance evaluation using i) Naive Bayes (purple), ii) Weighted Majority Vote (MV) (green), and iii) Simple Majority Vote (MV) (blue). On the left, results include all classification windows (1-6). On the right, results include the classification windows 1-5. The solid line represents the average subject results for the AB participants, while the dashed line corresponds to the performance of the TTA participant.

4. Discussion

The inherent challenge in our prediction task lies in the fact that all classes involved in the classification relate to walking on rigid ground. The distinguishing factor is whether the subsequent step occurs on a rigid, high, medium, or low-stiffness surface. The similarity between some of the cases (i.e., rigid with high stiffness and medium with low stiffness) introduces additional complexity into the prediction process, a challenge effectively addressed by ASTRA-BF, achieving a classification accuracy of up to 82%. Comparing our framework with a random choice classifier, which would yield a 25% prediction accuracy, we can confidently say the results of this work are particularly encouraging and important for the application of ASTRA-BF in the control architecture of powered lower-limb prostheses.

However, several limitations of the current study must be acknowledged. One limitation of this work lies in the fact that the outcomes of the present study primarily represent a participant pool comprising healthy adults. However, findings and results from the TTA participant strongly indicate that our framework can take into account the distinct EMG and kinematic parameters of each subject under the distinct stiffness conditions it is presented with. We, therefore, support that ASTRA-BF should be capable of producing comparable experimental results in a broader range of participants with TTA, including individuals with traumatic amputations among others. Additionally, while we acknowledge the limited diversity and size of the participant sample in this study, it is important to note that previous studies on lower limb prosthetics have also validated their frameworks using comparative population sizes [15, 48, 49, 6]. However, this small sample size, particularly the reliance on data from a single participant with LLA, might restrict the generalizability of the findings. A more diverse participant group, including individuals with different amputation types and varying activity levels, is thus needed to validate the robustness and applicability of the framework across broader populations.

Furthermore, while our study demonstrates the potential of the ASTRA-BF framework for individuals with LLA, the algorithm's real-time applicability to dynamically adjust prosthesis parameters, such as stiffness and torque, based on the predicted surface stiffness, has not been fully realized. This aspect of the framework—adjusting prosthesis control parameters in response to surface transitions—represents a critical next step in making the system more responsive and natural for users. Based on our previous works, we aim to utilize the prediction decision of the ASTRA-BF framework to switch from a standard prosthesis controller suitable for steady-state walking on even rigid terrains to an admittance controller specifically tailored for walking on compliant terrains [47]. ASTRA-BF has therefore been designed with real-time implementation in mind, using a lightweight ensemble of computationally efficient classifiers, in addition to implementing feature dimensionality reduction and a decision fusion strategy that minimizes per-frame computation.

In terms of future work, we plan to expand the participant pool to include a broader range of people with gait impairment, including individuals with traumatic amputations, as well as varying levels of amputation and activity levels. Additionally, integrating the predicted surface transition with adaptive control strategies for real-time adjustment of prosthesis parameters, such as stiffness, torque, and gait phase adjustments, is a key focus of ongoing research. This will allow for a more natural and safe walking experience by tailoring the prosthesis to varying terrains and dynamic walking conditions. We also plan to investigate the use of deep learning models and other advanced algorithms to improve prediction accuracy, particularly with larger and more diverse datasets. Overall, addressing these limitations and pursuing the outlined future directions will be essential for further strengthening the framework and its applicability in practical, real-world prosthetic control systems.

5. Conclusion

This paper significantly expands on an innovative pattern recognition algorithm designed to predict the user's intention to transition from a rigid to a compliant surface, utilizing EMG, kinematic, and kinetic data. The ASTRA-BF algorithm includes a significant extension of the previously proposed framework [24, 25] to multiple levels of compliant surfaces, as well as an expansion of the feature space utilized for prediction. Throughout this paper, additions, improvements, and adaptations of the existing framework achieved a 91% reduction in the number of selected features, as well as an 82% accuracy in the prediction of the user intent. Our classification strategy demonstrated robust and accurate predictions in both AB and TTA participants while maintaining a timely system response that is suitable for real-time implementations.

The outcomes of this study are particularly noteworthy, considering the classification involves distinguishing between four classes of surface stiffness. The fusion of EMG signals with kinematic and kinetic data led to successful predictions based solely on the user's intent to step on a rigid, high, medium, or low-stiffness surface. The examined levels of surface stiffness cover a wide range of surfaces found in real-world environments. ASTRA-BF holds potential for integration as part of a high-level controller, informing the prosthesis or lower extremity device and dynamically adjusting its parameters in real time. This advancement has the potential to enhance the robustness and safety of lower-limb prostheses and wearables, ultimately improving the quality of life for individuals with gait impairments, including those with LLA.

References

[1] K. A. Hawkins, D. J. Clark, C. K. Balasubramanian, E. J. Fox, Walking on uneven terrain in healthy adults and the implications for people after stroke hhs public access, NeuroRehabilitation 41 (2017) 765–774.

[2] B. J. Hafner, S. J. Morgan, D. C. Abrahamson, D. Amtmann, Characterizing mobility from the prosthetic limb user's perspective: Use of focus groups to guide development of the prosthetic limb users survey of mobility, Prosthetics and Orthotics International 40 (2016) 582–590.

[3] J. Kim, M. J. Major, B. Hafner, A. Sawers, Frequency and circumstances of falls reported by ambulatory unilateral lower limb prosthesis users: A secondary analysis, Physical Medicine and Rehabilitation 11 (2019) 344–353. doi:10.1016/J.PMRJ.2018.08.385.

[4] N. Thatte, H. Geyer, Toward balance recovery with leg prostheses using neuromuscular model control, IEEE transactions on bio-medical engineering 63 (2015) 904. doi:10.1109/TBME.2015.2472533.
URL `https://pmc.ncbi.nlm.nih.gov/articles/PMC4854805/`

[5] S. Sozzi, M. Schieppati, Balance adaptation while standing on a compliant base depends on the current sensory condition in healthy young adults, Frontiers in Human Neuroscience 16 (2022) 839799.

[6] M. J. MacLellan, A. E. Patla, Adaptations of walking pattern on a compliant surface to regulate dynamic stability, Experimental Brain Research 173 (2006) 521–530.

[7] D. P. Ferris, K. Liang, C. T. Farley, Runners adjust leg stiffness for their first step on a new running surface, Journal of Biomechanics 32 (1999) 787–794.

[8] H. Huang, F. Zhang, L. J. Hargrove, Z. Dou, D. R. Rogers, K. B. Englehart, Continuous locomotion-mode identification for prosthetic legs based on neuromuscular–mechanical fusion, IEEE Transactions on Biomedical Engineering 58 (2011) 2867.

[9] S. Huang, D. P. Ferris, Muscle activation patterns during walking from transtibial amputees recorded within the residual limb-prosthetic interface, Journal of NeuroEngineering and Rehabilitation 9 (2012) 1–16.

[10] L. Li, L. L. Ogden, Muscular activity characteristics associated with preparation for gait transition, Journal of Sport and Health Science 1 (2012) 27–35.

[11] J. A. Spanias, A. M. Simon, S. B. Finucane, E. J. Perreault, L. J. Hargrove, Online adaptive neural control of a robotic lower limb prosthesis, Journal of Neural Engineering 15 (2018) 016015.

[12] M. Liu, D. Wang, H. H. Huang, Development of an environment-aware locomotion mode recognition system for powered lower limb prostheses, IEEE transactions on neural systems and rehabilitation engineering : a publication of the IEEE Engineering in Medicine and Biology Society 24 (2016) 434–443.

[13] K. G. Rabe, T. Lenzi, N. P. Fey, Performance of sonomyographic and electromyographic sensing for continuous estimation of joint torque during ambulation on multiple terrains, IEEE Transactions on Neural Systems and Rehabilitation Engineering 29 (2021) 2635–2644.

[14] M. Liu, F. Zhang, H. H. Huang, An adaptive classification strategy for reliable locomotion mode recognition, Sensors (Basel, Switzerland) 17 (9 2017). doi:10.3390/S17092020.

[15] M. Cowan, S. Creveling, L. M. Sullivan, L. Gabert, T. Lenzi, A unified controller for natural ambulation on stairs and level ground with a powered robotic knee prosthesis, in: 2023 IEEE/RSJ International Conference on Intelligent Robots and Systems (IROS), 2023, pp. 2146–2151. doi:10.1109/IROS55552.2023.10341691.

[16] S. Cheng, C. A. Laubscher, R. D. Gregg, Controlling powered prosthesis kinematics over continuous transitions between walk and stair ascent, 2023 IEEE/RSJ International Conference on Intelligent Robots and Systems (IROS) (2023) 2108–2115.

[17] R. J. Cortino, T. K. Best, R. D. Gregg, Data-driven phase-based control of a powered knee-ankle prosthesis for variable-incline stair ascent and

descent, IEEE Transactions on Medical Robotics and Bionics (2023) 1–1.

[18] E. M. Glanzer, P. G. Adamczyk, Design and validation of a semi-active variable stiffness foot prosthesis, IEEE transactions on neural systems and rehabilitation engineering : a publication of the IEEE Engineering in Medicine and Biology Society 26 (2018) 2351. doi:10.1109/TNSRE.2018.2877962.

[19] M. K. Shepherd, E. J. Rouse, The vspa foot: A quasi-passive ankle-foot prosthesis with continuously variable stiffness, IEEE Transactions on Neural Systems and Rehabilitation Engineering 25 (2017) 2375–2386. doi:10.1109/TNSRE.2017.2750113.

[20] K. Reardon, Analyzing anticipatory muscle tensing as a measure of prospective action, Ph.D. thesis, College of William & Mary (2009).

[21] J. Skidmore, P. Artemiadis, On the effect of walking surface stiffness on inter-limb coordination in human walking: toward bilaterally informed robotic gait rehabilitation, Journal of NeuroEngineering and Rehabilitation 13 (2016) 32.

[22] E. Q. Yumbla, R. A. Obeng, J. Ward, T. Sugar, P. Artemiadis, Anticipatory muscle responses in transitions from rigid to compliant surfaces: towards smart ankle-foot prostheses, IEEE International Conference on Rehabilitation Robotics (2019) 880–885.

[23] M. Drolet, E. Q. Yumbla, B. Hobbs, P. Artemiadis, On the effects of visual anticipation of floor compliance changes on human gait: Towards model-based robot-assisted rehabilitation, Proceedings - IEEE International Conference on Robotics and Automation (2020) 9072–9078.

[24] C. Angelidou, P. Artemiadis, On predicting transitions to compliant surfaces in human gait via neural and kinematic signals, IEEE Transactions on Neural Systems and Rehabilitation Engineering 31 (2023) 2214–2223.

[25] C. Angelidou, P. Artemiadis, On intuitive control of ankle-foot prostheses: A sensor fusion-based algorithm for real-time prediction of transitions to compliant surfaces, 2023 IEEE/RSJ International Conference on Intelligent Robots and Systems (IROS) (2023) 2122–2127doi:10.1109/IROS55552.2023.10341783.

[26] A. Barkan, J. Skidmore, P. Artemiadis, Variable stiffness treadmill (VST): A novel tool for the investigation of gait, Proceedings - IEEE International Conference on Robotics and Automation (2014) 2838–2843.

[27] J. Skidmore, A. Barkan, P. Artemiadis, Variable stiffness treadmill (VST): System development, characterization, and preliminary experiments, IEEE/ASME Transactions on Mechatronics 20 (2015). doi:10.1109/TMECH.2014.2350456.

[28] V. Chambers, B. Hobbs, W. Gaither, A. Zhou, C. Karakasis, P. Artemiadis, The variable stiffness treadmill 2: Development and validation of a unique tool to investigate locomotion on compliant terrains, Journal of Mechanisms and Robotics 17 (3) (2025).

[29] C. L. Brockett, G. J. Chapman, Biomechanics of the ankle, Orthopaedics and Trauma 30 (2016) 232–238.

[30] H. J. Hermens, B. Freriks, C. Disselhorst-Klug, G. Rau, Development of recommendations for semg sensors and sensor placement procedures, Journal of Electromyography and Kinesiology 10 (2000) 361–374.

[31] Vicon Motion Systems, Plug-in gait reference guide, `https://help.vicon.com/space/Nexus216/11607059/Plug-in+Gait+Reference+Guide`.

[32] C. Karakasis, P. Artemiadis, F-VESPA: A kinematic-based algorithm for real-time heel-strike detection during walking, IEEE International Conference on Intelligent Robots and Systems (2021) 5098–5103.

[33] B. Hobbs, P. Artemiadis, A systematic method for outlier detection in human gait data, in: International Conference on Rehabilitation Robotics (ICORR), 2022.

[34] G. Wang, Q. Li, L. Wang, W. Wang, M. Wu, T. Liu, Impact of sliding window length in indoor human motion modes and pose pattern recognition based on smartphone sensors, Sensors 2018, Vol. 18, Page 1965 18 (2018) 1965.

[35] B. Hudgins, P. Parker, R. N. Scott, A new strategy for multifunction myoelectric control, IEEE Transactions on Biomedical Engineering 40 (1993) 82–94.

[36] F. Hu, M. Qian, K. He, W. A. Zhang, X. Yang, A novel multi-feature fusion network with spatial partitioning strategy and cross-attention for armband-based gesture recognition, IEEE Transactions on Neural Systems and Rehabilitation Engineering (2024). doi:10.1109/TNSRE.2024.3487216.

[37] R. B. Azhiri, M. Esmaeili, M. Jafarzadeh, M. Nourani, Emg signal classification using reflection coefficients and extreme value machine, BioCAS 2021 - IEEE Biomedical Circuits and Systems Conference, Proceedings (2021).

[38] X. Jiang, C. Napier, B. Hannigan, J. J. Eng, C. Menon, Estimating vertical ground reaction force during walking using a single inertial sensor, Sensors (Basel, Switzerland) 20 (2020) 1–13. doi:10.3390/S20154345.

[39] W. Yang, K. Wang, W. Zuo, Neighborhood component feature selection for high-dimensional data, Journal of Computers 7 (2012) 162–168.

[40] C. Angelidou, P. Artemiadis, Reducing complexity, enhancing precision: Predicting compliant surface transitions in walking via neighborhood component analysis, in: 10th IEEE RAS/EMBS International Conference on Biomedical Robotics and Biomechatronics (BioRob), 2024.

[41] N. V. Chawla, K. W. Bowyer, L. O. Hall, W. P. Kegelmeyer, SMOTE: Synthetic minority over-sampling technique, Journal of Artificial Intelligence Research 16 (2002) 321–357.

[42] R. Blagus, L. Lusa, SMOTE for high-dimensional class-imbalanced data, BMC bioinformatics 14 (3 2013).

[43] G. F. M. de Souza, A. C. Netto, A. H. de Andrade Melani, M. A. de Carvalho Michalski, R. F. da Silva, Engineering systems' fault diagnosis methods, Reliability Analysis and Asset Management of Engineering Systems (2022) 165–187.

[44] S. Farhadpour, T. Warner, A. Maxwell, Selecting and interpreting multiclass loss and accuracy assessment metrics for classifications with class imbalance: Guidance and best practices, Remote Sensing 16 (2024) 533. doi:10.3390/rs16030533.

[45] H. Sadeghi, P. Allard, M. Duhaime, Muscle power compensatory mechanisms in below-knee amputee gait, American Journal of Physical Medicine and Rehabilitation 80 (2001) 25–32.

[46] N. T. Pickle, A. M. Grabowski, J. R. Jeffers, A. K. Silverman, The functional roles of muscles, passive prostheses, and powered prostheses during sloped walking in people with a transtibial amputation, Journal of Biomechanical Engineering 139 (11 2017).

[47] C. Karakasis, R. Salati, P. Artemiadis, Adjusting the quasi-stiffness of an ankle-foot prosthesis improves walking stability during locomotion over compliant terrain, IEEE/RSJ International Conference on Intelligent Robots and Systems (IROS) (2023) 2140–2145.

[48] A. Fleming, W. Liu, H. Huang, Neural prosthesis control restores near-normative neuromechanics in standing postural control, Science Robotics 8 (10 2023). doi:10.1126/scirobotics.adf5758.

[49] J. Mendez, S. Hood, A. Gunnel, T. Lenzi, Indirect volitional swing control allows for level-ground walking and crossing over obstacles with a powered knee and ankle prosthesis, Science robotics 5 (7 2020). doi:10.1126/SCIROBOTICS.ABA6635.